Mechanisms for composite particle production in nuclear reactions using $(\alpha,\alpha' x)$ reactions up to 40 MeV/nucleon

H. Machner
Institut für Kernphysik, Kernforschungsanlage Jülich, D-5170 Jülich, West Germany and Universität Bremen, FB Physik, D-2800 Bremen 33, West Germany

U. Bechstedt, A. Djaloeis, and P. Jahn
Institut für Kernphysik, Kernforschungsanlage Jülich, D-5170 Jülich, West Germany
(Received 30 October 1981)

Spectra of α particles from 90, 120, and 160 MeV α-induced reactions on ^{54}Fe have been measured and, together with data taken at 59 MeV, were analyzed in terms of the exciton coalescence model. Multiple-particle emission was found to be important in reproducing the shapes of the angle integrated spectra. Deduced radii P_0 of coalescence spheres in momentum space are consistent with the assumption that P_0 is constant.

[NUCLEAR REACTIONS ^{54}Fe$(\alpha,\alpha' x)$, $E=59$, 90, 120, 160 MeV; measured $\sigma(\epsilon,\vartheta)$, $\sigma(\epsilon)$; exciton coalescence model analysis, thermodynamics of light nuclei production.]

I. INTRODUCTION

The emission of particles following the interaction of a projectile with a target nucleus constitutes a large fraction of the total reaction cross section and is thus of fundamental importance. The products emitted are primarily nucleons and light composite particles such as deuterons, tritons, and helium nuclei. In the case of α particles this emission may be due to preformed clusters, but it is unlikely that knockout of preformed deuterons, tritons, or ^{3}He particles will significantly contribute to the observed production cross sections. Theories have been formulated, moreover, to describe the formation of clusters including α particles. These theories are based on differing physical assumptions.

(a) The coalescence model[1-3] is a purely statistical model. Complex particle formation from "excited nucleons" (excited with respect to the Fermi surface of the nucleus) is treated in a final-state interaction description. A mean field (represented by the total potential) acts as a third body necessary for energy and momentum conservation.

(b) The equilibrium approach[4]—a statistical thermodynamical model—assumes that thermal equilibrium, both kinetic and chemical, is achieved during the collision of projectile and target.

(c) The sudden approximation model[5] assumes that complex particle formation occurs during the expansion of a fireball. During this expansion a fast transition from a strongly interacting phase to a weakly interacting one should take place. The probability of forming clusters is related to the overlap of wave functions before and after the transition.

By comparing the different models[2-5] one finds that the power-law relationship between the momentum-space density of an emitted nucleus and the appropriate power of the nucleon momentum-space density is similar. The models differ in the dependence of the momentum-space radius P_0 on the excitation energy of the emitting volume. The study of the energy dependence of P_0 seems, therefore, to be a useful tool to gain insights regarding the validity of different models. The authors of Ref. 6 have already studied the reactions ^{20}Ne+NaF and ^{20}Ne+^{208}Pb with bombarding energies of 400, 800, and 2100 MeV/nucleon and have measured p, d, t, and ^{3}He spectra. The composite particle spectra have been well reproduced by calculated spectra when approximating excited cascade nucleons by the observed proton spectra. This procedure yields constant P_0 values. However, the number of nucleons emitted in clusters is not negligible at these high excitation energies. It is therefore necessary to add these nucleons to the proton and neutron spectra to get intermediate or primordial nucleon distributions. The striking agreement between data and calculation is not obtained when the observed proton spectra are modified to take into account such depletion effects.[6] Similar observations have been made by Gosset *et al.*[7]

In a recent approach intermediate nucleon distributions are calculated, thus avoiding the problems discussed above. This approach is successful at moderate energies of some tens of MeV/nucleon. We therefore have measured the energy dependence of ^{54}Fe(α,$\alpha'x$) reactions up to an α energy of 160 MeV. In the following section the details of our measurements are presented. The exciton coalescence model (ECM) (Ref. 8) is then extended to the high energies. Finally, we compare our results with model predictions.

II. EXPERIMENTS AND RESULTS

A. Experimental procedure

The α-particle spectra from reactions induced by 90, 120, and 160 MeV α particles from the unanalyzed external beam of the isochronous cyclotron JULIC have been measured. The beam energy resolution ($\Delta E/E \simeq 0.003$) was sufficient for an investigation of the continuous spectra, and the energy resolution of the spectra observed was better than 1% depending on the beam energy and the target thicknesses. The experimental setup was checked by taking spectra with no target in the target frame, thus making sure that there were no background problems. The total number of events was always less than 1000 counts/s, thus reducing pileup and dead-time effects to a negligible level. By means of a pair of quadrupole magnets, the beam was focused and centered on the target to a beam spot of 4 by 2 mm. The beam was then again focused to the Faraday cup with another quadrupole doublet. A Ge(Li) monitor counter was also used as a redundancy check on the charge integration.

Self-supporting metallic foils of enriched ^{54}Fe (96.8% isotopically pure) with thicknesses of 15.7 mg/cm^2 served as targets for the bombardments at 90 and 120 MeV, while a 1.2 mg/cm^2 foil was used in the 160 MeV experiments. The targets were mounted on the target ladder which was located in the center of a scattering chamber of $\sim$1 m diameter. Charged reaction products were detected using ΔE-E telescopes. The ΔE counter was, in all cases, a Si surface barrier detector. In the experiment using the 90 MeV beam a stack of three 2000 μm Si surface barrier counters served as the E detector, while at 120 MeV a 5 mm Si surface barrier counter (at 30° to the incident particles) and at 160 MeV a Ge(Li) (Ref. 9) were used. All data concerning the conditions of the three experiments are listed in Table I. A pair of tantalum collimators was used as an antiscattering aperture and to define the solid angle. The telescopes were connected to a fast electronic particle identification system (Canberra 2161) using the Bethe-Bloch relation. Alpha-particle spectra were accumulated in a pulse height analyzer and recorded on magnetic tape. Energy calibration of the spectra was performed with a polyethylene (CH_2) target from which elastically and inelastically scattered α particles on ^{12}C, elastic scattered α particles on protons, as well as recoiling protons, were detected.

Since the uncertainties in the cross sections resulting from energy calibration are negligible, the uncertainties in the target thicknesses (about 15%) are the main contribution to the systematic error. The uncertainties in the solid angles are less than 1%, and charge integration is estimated to be correct within 2%. The statistical error depends on the measuring angle. Typical values are 2% at forward angles and 10% at backward angles.

B. Experimental results

Figures 1–3 show inelastic α-particle (α') spectra from the bombardment of ^{54}Fe with α particles of

TABLE I. Experimental setup.

Beam energy (MeV)	Target thickness (mg/cm^2)	Detector thicknesses ΔE (μm)	E (mm)	$\Delta\Omega$ (msr)	$\Delta\vartheta$	ϑ_{min}	ϑ_{max}	Number of angles measured
90	15.7	235	6[a]	0.50	1.0°	15°	140°	10
120	15.7	232	5.8[b]	0.68	1.2°	10°	160°	11
160	1.2	1000	Ge(Li)	0.19	0.9°	15°	135°	7

[a] 3×2000 μm.
[b] 5 mm counter turned by 30°.

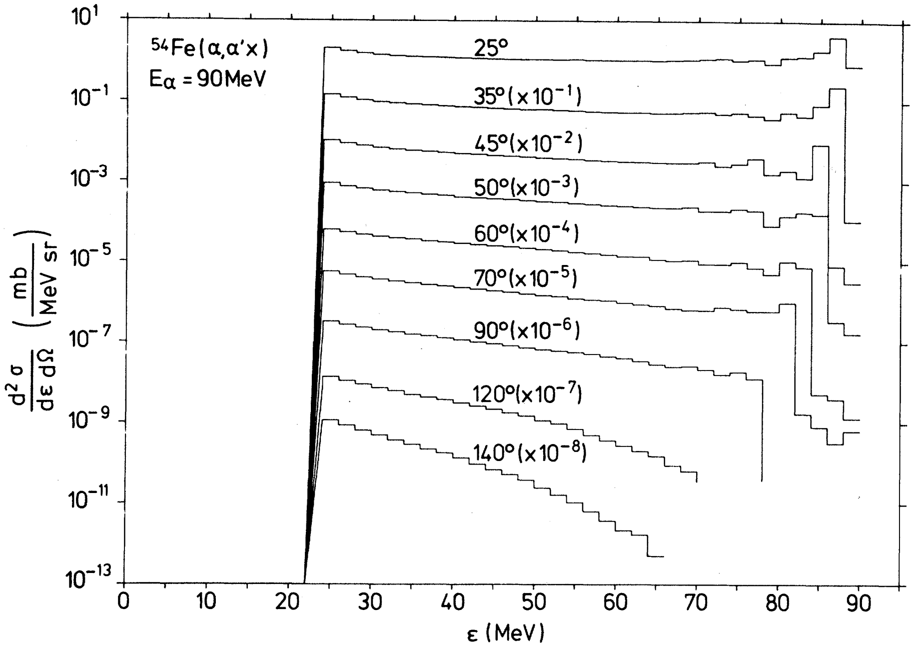

FIG. 1. Spectra of α' particles from α-induced reactions on ^{54}Fe at $E_\alpha=90$ MeV.

90, 120, and 160 MeV. The laboratory angle is indicated next to the appropriate curve. The cross sections were deduced by averaging over 2 MeV wide energy bins, thus improving the statistics. In the forward angle spectra at α' energies below the elastic peak, a flat and structureless region appears. Backward-angle spectra show a steep structureless shape. From these data, angle-integrated cross sections were obtained by approximating the integral by a sum. The angle-integrated cross sections are shown later where they are compared with calculations. It is interesting to note that the height of the

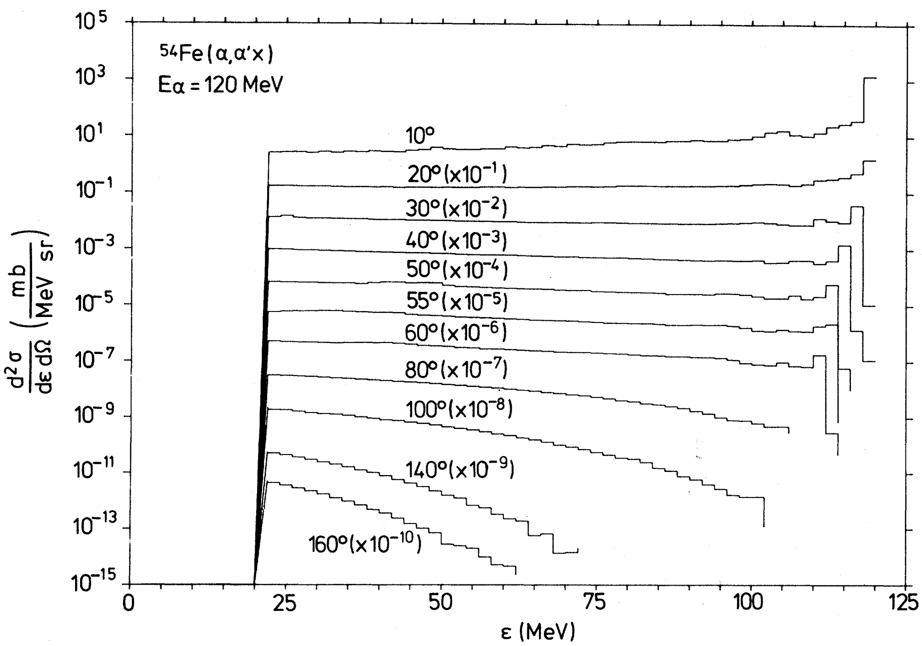

FIG. 2. As in Fig. 1, but for $E_\alpha=120$ MeV.

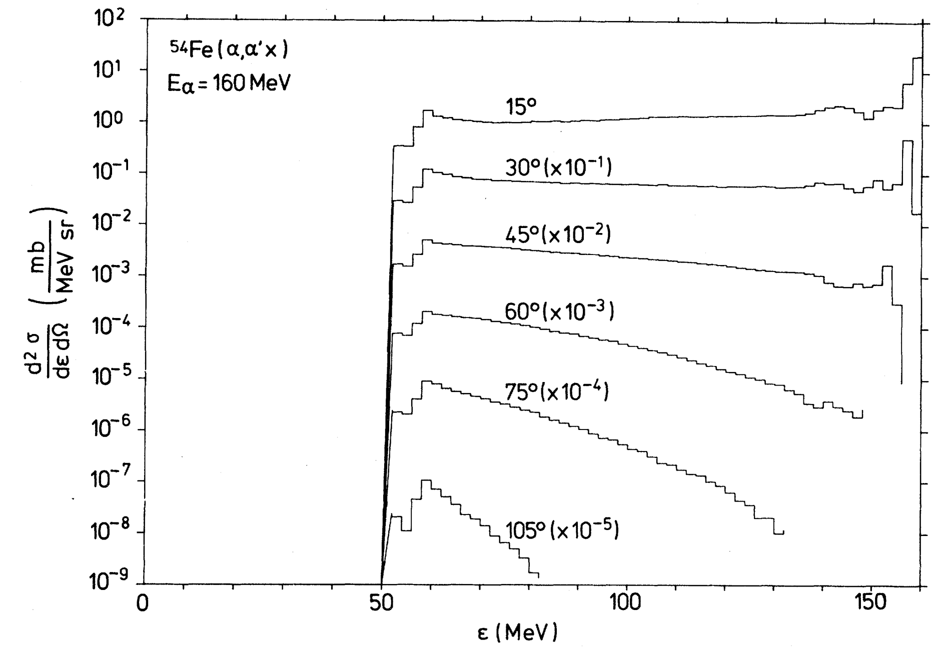

FIG. 3. As in Fig. 1, but for $E_\alpha = 160$ MeV.

bump at ~ 17 MeV excitation energy, resulting from excitation of the giant quadrupole resonance in ^{54}Fe, increases with bombarding energy.

III. DESCRIPTION OF THE MODELS

A. Exciton coalescence model

In this section the emission of α particles in the framework of the ECM (Ref. 8) is briefly described. The basis of the ECM is that complex particle formation occurs from excited nucleons with small transverse momenta. It is assumed that, for example, a proton and a neutron coalesce into a deuteron if the second nucleon is within a sphere in momentum space with radius P_0 around the momentum P_c of the first nucleon. The distributions of the excited particles (p) and holes (h) with respect to the Fermi energy are governed by a generalized master equation[10]

$$\frac{\partial P(n,t)}{\partial t} = \sum_m \int d\Omega' \lambda(m \to n, \Omega' \to \Omega) P(m,\Omega',t) - P(n,\Omega,t)\Big[\sum_i \lambda_c^i(n,E) + \sum_m \int d\Omega' \lambda(n \to m, \Omega \to \Omega')\Big] . \tag{1}$$

The intermediate states are classified according to their number of excitons ($n = p + h$) and the direction $\Omega(\vartheta,\varphi)$ of a scattered particle. $P(n,\Omega,t)$ denotes the occupation probability of the states (n,Ω) at time t, while the averaged transition rates are given by λ. Angle integration leads to the angle-independent master equation. If we restrict ourselves to only two-body interactions ($\Delta n = \pm 2$), this equation reads:

$$\frac{\partial P(n,t)}{\partial t} = \lambda_-(n+2,E)P(n+2,t) + \lambda_+(n-2,E)P(n-2,t) - \Big[\lambda_+(n,E) + \lambda_-(n,E) + \sum_i \lambda_c^i(n,E)\Big]P(n,t) ,$$
$$P(n,t=0) = \delta_{nn_0} . \tag{2}$$

The emission rate λ_c^i must be extended over all exit channels i. For the reactions under discussion here, it is sufficient, in practice, to take only proton and neutron emission into account. The transition from Eq. (1) to (2) is, for example, valid for the factorization ansatz

$$\int_0^{t_{\rm equ}} P(n,\Omega,t)dt = A(n,\Omega)\int_0^{t_{\rm equ}} P(n,t)dt = A(n,\Omega)\tau(n,E) \tag{3}$$

if the relation

$$\int A(n,\Omega)d\Omega = 1 \tag{4}$$

holds. The angular distribution functions have been derived from the recurrence relation[11]

$$A(n+2,\Omega)=\int d\Omega' A(n,\Omega')W(\Omega'\to\Omega) \qquad (5)$$

with the transition rate W calculated from the free nucleon-nucleon cross section

$$W(\Omega'\to\Omega)\propto \frac{dG_{NN}}{d\Omega}(\Omega'\to\Omega)\ . \qquad (6)$$

The initial condition for infinite nuclear matter is given by

$$A(n_0,\Omega(\vartheta,\varphi))=\pi^{-1}\cos\vartheta\,\Theta(\pi/2-\vartheta) \qquad (7)$$

with the step function Θ.

The emission probability for a particle of type i with energy ϵ_i from a state with p particles and h holes is given by[12]

$$W_i(p,h,\epsilon_i)=\frac{2S_i+1}{\pi^2\hbar^3}\mu_i\epsilon_i\sigma^i_{inv}(\epsilon_i) \times F(p,h,p_i,E,\epsilon_i)\gamma_i\ . \qquad (8)$$

Here, all factors except the last two are the same as in the statistical model. The quantity F denotes the probability of having p_i particles with energy ϵ_i+B_i (B_i = binding energy) in unbound states

$$F(p,h,p_i,E,\epsilon_i)=\frac{\rho(p-p_i,h,E-B_i-\epsilon_i)}{\rho(p,h,E)} \times\frac{\rho(p_i,0,B_i+\epsilon_i)}{g}p\begin{pmatrix}p\\p_i\end{pmatrix}^{-1}, \qquad (9)$$

where $\rho(p,h,E)/g$ gives the number of ways to distribute E energy quanta on $p+h$ excitons and g is the single-particle level density

$$\rho(p,h,E)=\frac{g^{p+h}E^{p+h-1}}{(p+h-1)!p!h!}\ . \qquad (10)$$

However, it should be noted that, if the binding energy is neglected, integration yields

$$\int_0^E F(p,h,p_i,E,\epsilon_i)d\epsilon_i=p\ . \qquad (11)$$

The last factor in Eq. (8), γ_i, denotes the fraction of those states where the p_i particles are coalesced into a cluster of type i. The coalescence radius mentioned above is obtained from[8]

$$\gamma_i=\gamma_{x+y}=[\tfrac{4}{3}\pi(P_0/uc)^3]^{x+y-1}\ , \qquad (12)$$

with x (y) being the number of protons (neutrons) in the cluster i, u giving the nucleon mass, and c denoting the velocity of light.

The cross section can be then approximated[8] as

$$\frac{d^2\sigma_i(\epsilon,\vartheta)}{d\epsilon\, d\Omega}=\sigma_0\sum_{\substack{n=n_0(i)\\ \Delta n=2}}^{\bar n} W_i(p,h,\epsilon) \times A(n,\Omega)\tau(n,E)\ , \qquad (13)$$

where σ_0 is the total reaction cross section derived from the optical model. The summation is extended from n_0, the projectile and ejectile dependent initial exciton number,[8,12] up to $\bar n$, the exciton number of statistical equilibrium. This number is obtained from the condition $\lambda_+(\bar n,E)=\lambda_-(\bar n,E)$.

B. Multiple precompound particle emission

At the high energies under discussion here the residual nucleus with excitation energy $U=E-\epsilon_i-B_i$ might have enough energy to emit a second particle p_j during the precompound phase. This process can be described again by a master equation

$$\frac{\partial Q(m,t)}{\partial t}=\lambda_+(m-2,U)Q(m-2,t)+\lambda_-(m+2,U)Q(m+2,t) -[\lambda_+(m,U)+\lambda_-(m,U)+\sum_k \lambda_c^k(n,U)]Q(m,t) \qquad (14)$$

with the initial condition

$$Q(m,t=0)=\delta(m,m_0=p-p_i+h)W_i(p,h,\epsilon_i)\tau(n,E)\ . \qquad (15)$$

The quantity Q denotes the occupation probability of an m-exciton state at time t.

The emission rate is given by

$$W_j(p,h,p_i,E,U,\epsilon_j)=\frac{2S_j+1}{\pi^2\hbar^3}\mu_j\epsilon_j\sigma^j_{inv}(\epsilon_j)F(p-p_i,h,p_j,U,\epsilon_j)\gamma_j\ , \qquad (16)$$

where all quantities have the same meaning as above. From Eq. (14) one can calculate the lifetime

$$\bar{\tau}(m,U)=\int_0^{t_{\text{equ}}} Q(m,t)dt \tag{17}$$

thus leading to the cross section

$$\frac{d\sigma_{ij}(\epsilon_j)}{d\epsilon}=\sigma_0 \sum_{\substack{n=n_0(i)\\ \Delta n=2}}^{\bar{n}} \sum_{\substack{m=m_0(n,p_i)\\ \Delta m=2}}^{\bar{n}} \int_0^{E-B_i} dU\, W_j(p,h,p_i,E,U,\epsilon_j)\bar{\tau}(m,U) . \tag{18}$$

The total angle-integrated cross section for a particle type j is then given by

$$\frac{d\sigma}{d\epsilon}=\frac{d\sigma_j}{d\epsilon}+\sum_i \frac{d\sigma_{ij}}{d\epsilon} . \tag{19}$$

C. Comparison of the ECM with the coalescence model

A common feature of the coalescence model (CM) (Ref. 3) and ECM (Ref. 8) is the equation for the cross section

$$\frac{d^2\sigma}{d\epsilon\, d\Omega}=\sigma_0(\tfrac{4}{3}\pi P_0{}^3)^{x+y-1} f_i(\vec{p}) , \tag{20}$$

where $\vec{p}$ represents the nucleon momentum and $f_i(\vec{p})$ is the model dependent distribution of the cascade nucleons. In ECM, $f_i(\vec{p})$ is given by the sum over nucleon distributions in possible exciton states. In CM (for high nucleon multiplicities) $f_i(\vec{p})$ is given by[3]

$$f_i(\vec{p})=\left[\frac{1}{\sigma_0}\frac{d^2\sigma_N}{p^2 dp\, d\Omega}\right]^{x+y}\frac{1}{x!y!} . \tag{21}$$

The cascade nucleon distributions are then approximated by the observed proton spectra $d^2\sigma_N/p^2dp\,d\Omega$.

As noted in Ref. 8, the application of this approximation does not seem to be appropriate for the energy regime under discussion here. The multiplicity of the excited nucleons is small. Proton spectra do not reflect nucleon distributions due to superposition of evaporated protons from the compound nucleus and Coulomb distortion effects. However, using the angular distribution of protons from the evaporation peak of 59 MeV α-induced reactions as input for CM [Eqs. (20) and (21)] an excellent fit of the nonevaporative α-particle angular distribution is obtained (see Fig. 4). The same degree of agreement can be obtained for all energies, but for each energy the coalescence radius P_0 must be fitted (Figs. 5 and 6). The minima in Figs. 5 and 6 coincide with the evaporation maxima of the proton spectra. Even though the above procedure yields excellent fits (Figs. 4–6) it is unlikely that compound protons can coalesce into α particles or deuterons which are responsible for the high-energy component of the spectra. This result can be understood, if both eva-

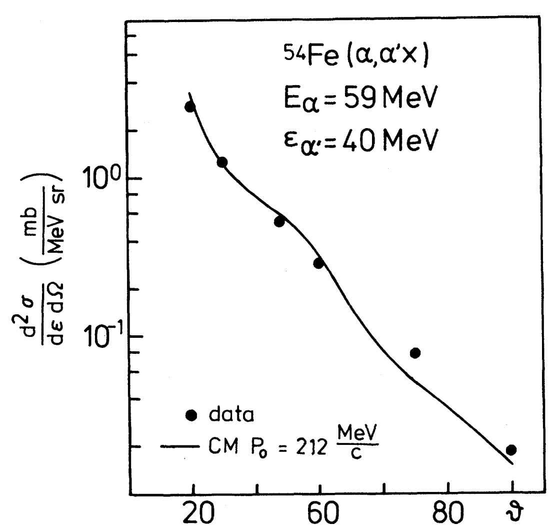

FIG. 4. Angular distributions for the ^{54}Fe(α,$\alpha'x$) reactions at E_α=59 MeV and $\epsilon_{\alpha'}$=40 MeV. The dots represent the experimental data. The solid curve connects the calculated points from CM. The data are from Ref. 13.

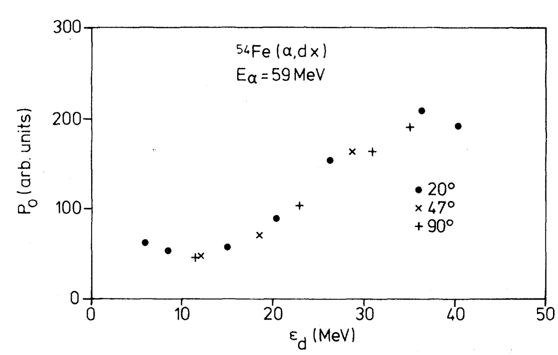

FIG. 5. Extracted P_0 values for the ^{54}Fe(α,dx) reaction at E_α=59 MeV for various ϵ_d and emission angles using CM and data from Ref. 13.

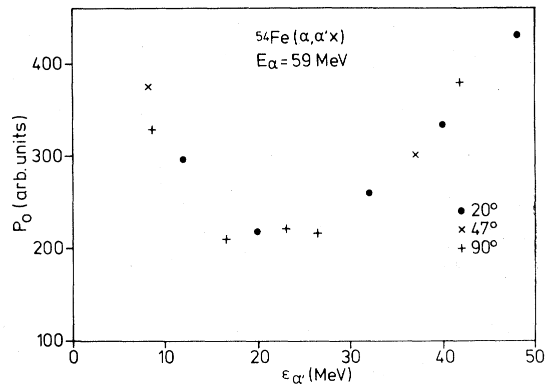

FIG. 6. As in Fig. 5, but for the ^{54}Fe($\alpha,\alpha'x$) reaction.

porated protons from the compound nucleus as well as precompound protons have the same angular distribution. It therefore seems necessary to use calculated nucleon spectra when applying CM.

IV. COMPARISON WITH MODEL CALCULATIONS

Calculations have been carried out for bombarding energies of 59, 90, 120, and 160 MeV. To compare calculations at the smallest bombarding energy, data from Ref. 13 have been used. In Figs. 7–10 contributions to the cross sections from different exciton states labeled by the number of interactions are shown. Here we compare calculations for a bombarding energy of 59 MeV (Figs. 7 and 8) with those for a higher bombarding energy

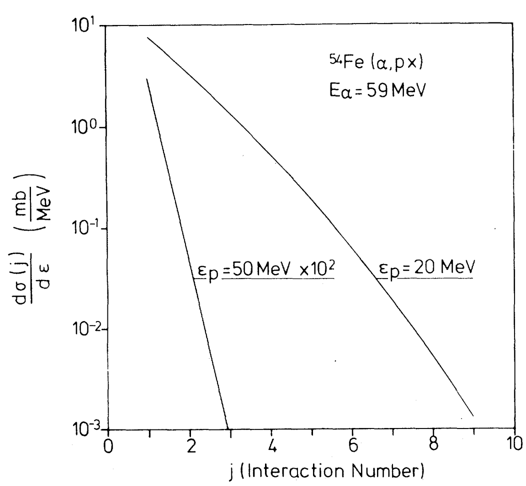

FIG. 7. Dependence of the partial cross section $d\sigma(j)/d\epsilon$ on the interaction number j for the ^{54}Fe(α,px) reaction at $E_\alpha = 59$ MeV.

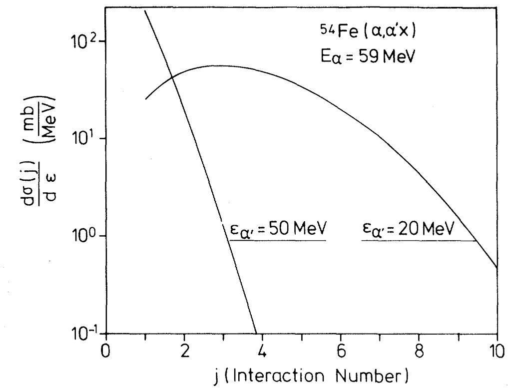

FIG. 8. As in Fig. 7, but for the ^{54}Fe($\alpha,\alpha'x$) reaction.

of 160 MeV (Figs. 9 and 10). Common to all calculations is the fact that for emitted particles at high energy nearly the total cross section comes from the contribution of the first step. This fact is more pronounced for the higher bombarding energy. For α' particles in the exit channel (Figs. 8 and 10) the importance of higher collision numbers clearly emerges. This may have its origin in the fact that, after a series of collisions, a large number of excited particles exist. Thus, the probability of having a cluster from coalescing nucleons is increased.

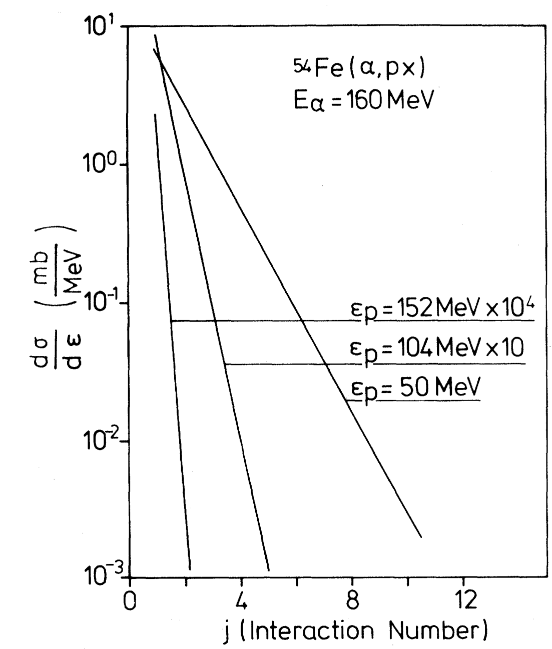

FIG. 9. As in Fig. 7, but for $E_\alpha = 160$ MeV.

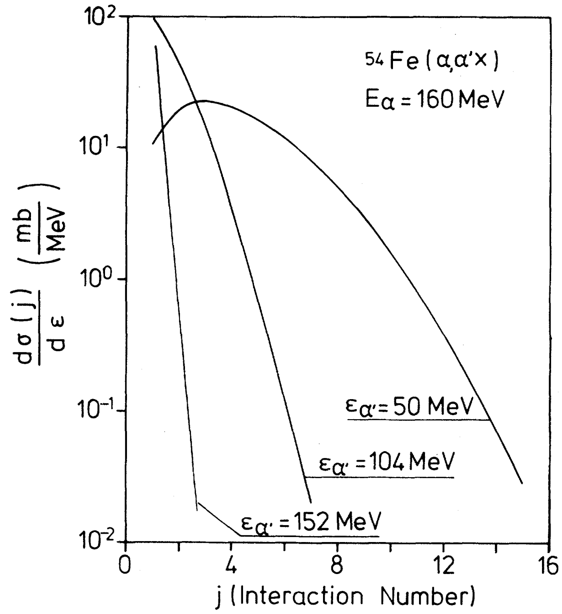

FIG. 10. As in Fig. 8, but for $E_\alpha = 160$ MeV.

This finding agrees well with observations from a rapidity plot (Fig. 11) for the 120 MeV data. In this figure, Galilei invariant cross sections are plotted as contour lines dependent on $v_{||}$, the velocity parallel to the beam axis, and $v_\perp$, the velocity perpendicular to it. The emission pattern in such a diagram from a source which emits particles isotropic in its rest frame are concentric semicircles around the source velocity v_s. Large cross sections measured at backward angles and small cross sections at forward angles are on concentric semicircles around a value v_S. Evaporation from the compound nucleus is expected to result in concentric semicircles around v_{CN}. The beam velocity is indicated as v_p. Assuming a two-body interaction and linear momentum conservation yields, from the obtained value $v_S = 3$ $(\mathrm{MeV}/u_0)^{1/2}$ (u_0=nucleon mass in units of MeV/c^2), an emitting source with ≈ 10 nucleons. The average for these cross sections from ECM calculation is nine excited nucleons for the first chance emission, which is in good agreement with the above calculations. Larger cross sections at forward angles—which may originate from the first interactions—do not show a clear center for semicircles. The emission volume responsible for these cross sections has a velocity between v_S and v_P. From these observations it seems reasonable to assume α emission from a source moving with velocity v_S parallel to the beam. This source emits particles isotropically in its rest frame. Transforming

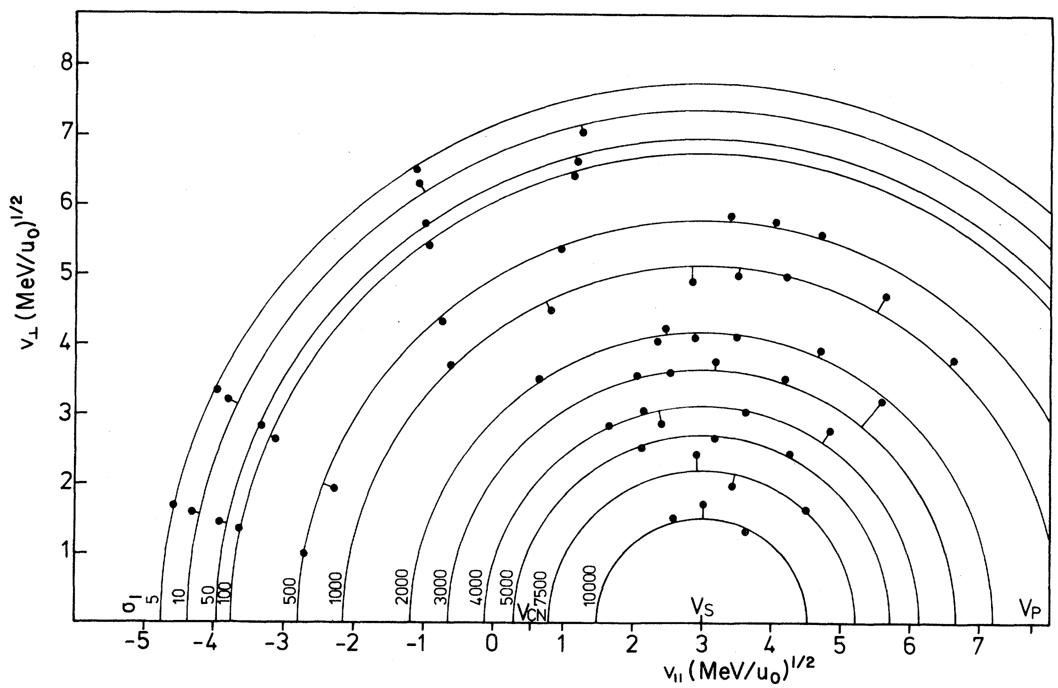

FIG. 11. Rapidity plot for the ^{54}Fe$(\alpha,\alpha'x)$ reactions at $E_\alpha = 120$ MeV. The quantity u_0 denotes the nucleon mass. The Galilei invariant cross sections in units of 10^5 mb/sr MeV $(\mathrm{MeV}\,u_0)^{-1/2}$ (dots) are shown as a contour plot. These cross sections tend to follow concentric semicircles around v_s. The velocity parallel to the beam axis is denoted by $v_{||}$ and the velocity perpendicular to the beam axis by $v_\perp$. The compound nucleus velocity (V_{CN}) is indicated as well as the projectile velocity (v_p).

TABLE II. Parameters obtained from ECM analysis.

E_α (MeV)	γ_α	P_0 (MeV/c)	$\tilde{P}_0$ (MeV/c)[a]	R (fm)[b]
59	10.43×10^{-3}	351	301	1.59
90	7.52×10^{-3}	338	290	1.65
120	8.33×10^{-3}	342	283	1.63
160	6.24×10^{-3}	331	284	1.68

[a]The reduced radii are calculated (Ref. 4) as

$$\tilde{P}_0{}^3=P_0{}^3\left[\frac{2^{x+y}}{(2S+1)(x+y)^3}\right]^{1/(x+y-1)} .$$

[b]The radii are deduced from $\tilde{P}_0$ using the phase space relation.

the data into this system (primed quantities) and assuming further a Maxwellian distribution leads to

$$\frac{d^2\sigma'}{d\epsilon'\,d\Omega'}=0.167\sqrt{\epsilon'}\times\exp[-\epsilon'/28.2\text{ MeV}]\frac{\text{mb}}{\text{MeV sr}} . \quad (22)$$

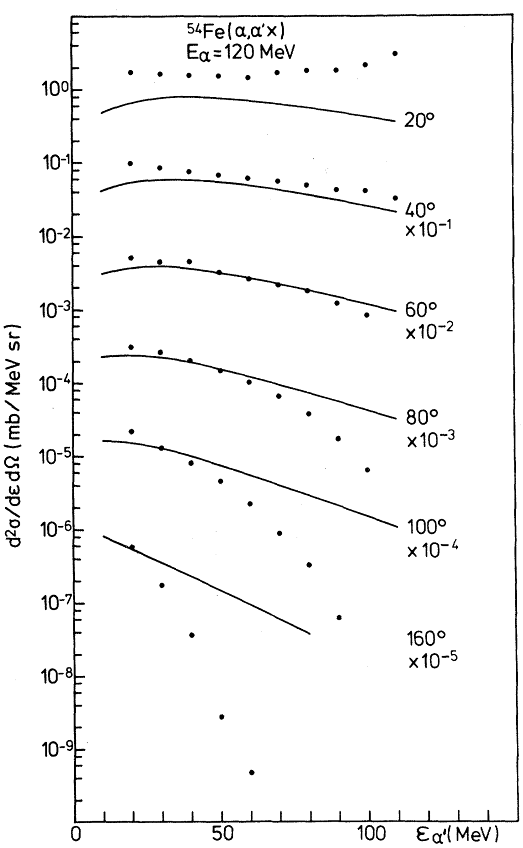

FIG. 12. Comparison of selected experimental ^{54}Fe($\alpha,\alpha'x$) spectra for $E_\alpha=120$ MeV (dots) with emission from a moving equilibrated source (solid line).

It is shown in the Appendix that complex particle emission reflects, within the framework of CM, the same features of the source, such as its temperature and velocity, as does nucleon emission. We have compared angle-integrated spectra from Eq. (22) with CM calculations [Eqs. (21) and (22)] using angle-independent exciton model calculations for proton emission. Such a comparison yields $P_0=345$ MeV/c, which is in excellent agreement with the ECM result of the same data, i.e., $P_0=342$ MeV/c (see Table II).

However, the very high value of 28.2 MeV for the temperature of the source with respect to the total excitation energy of 120 MeV is surprising. Transformation of (22) into the laboratory system gives satisfactory results only at fairly low α-particle energies and angles which are not far forward or backward (Fig. 12). This is just the region

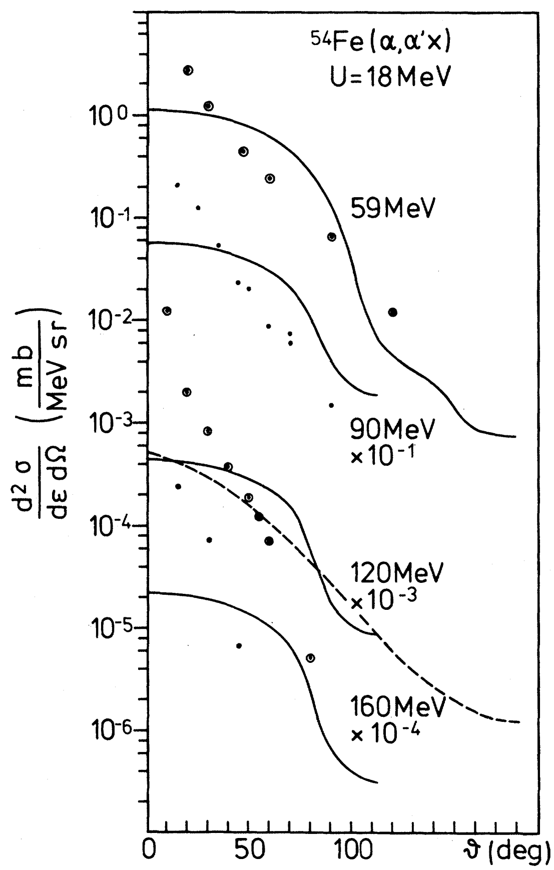

FIG. 13. Comparison of the experimental ^{54}Fe($\alpha,\alpha'x$) angular distributions (dots) for $U=18$ MeV with the ECM predictions (solid line). The initial angular distribution $A(n_0,\Omega)$ is according to Eq. (7). Emission from a moving equilibrated source is given as a dashed line.

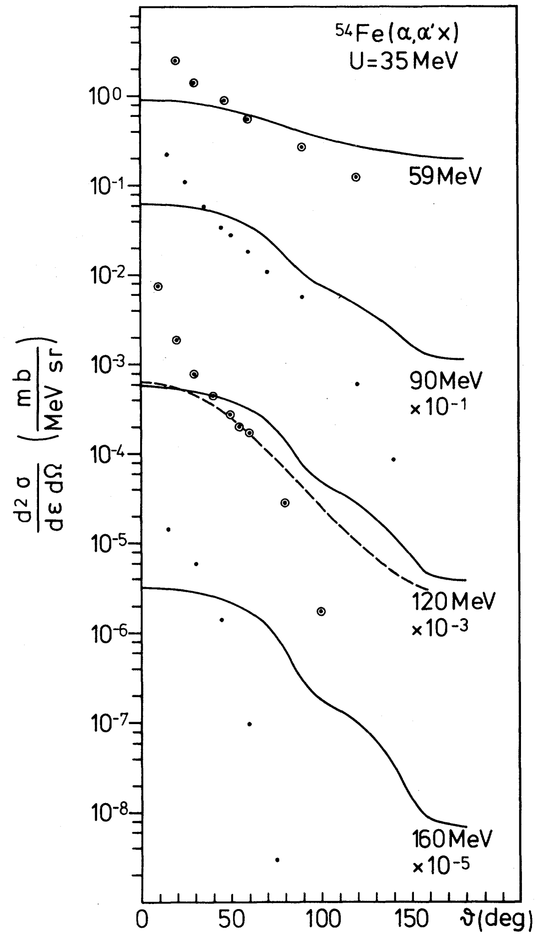

FIG. 14. As in Fig. 13, but for $U=35$ MeV.

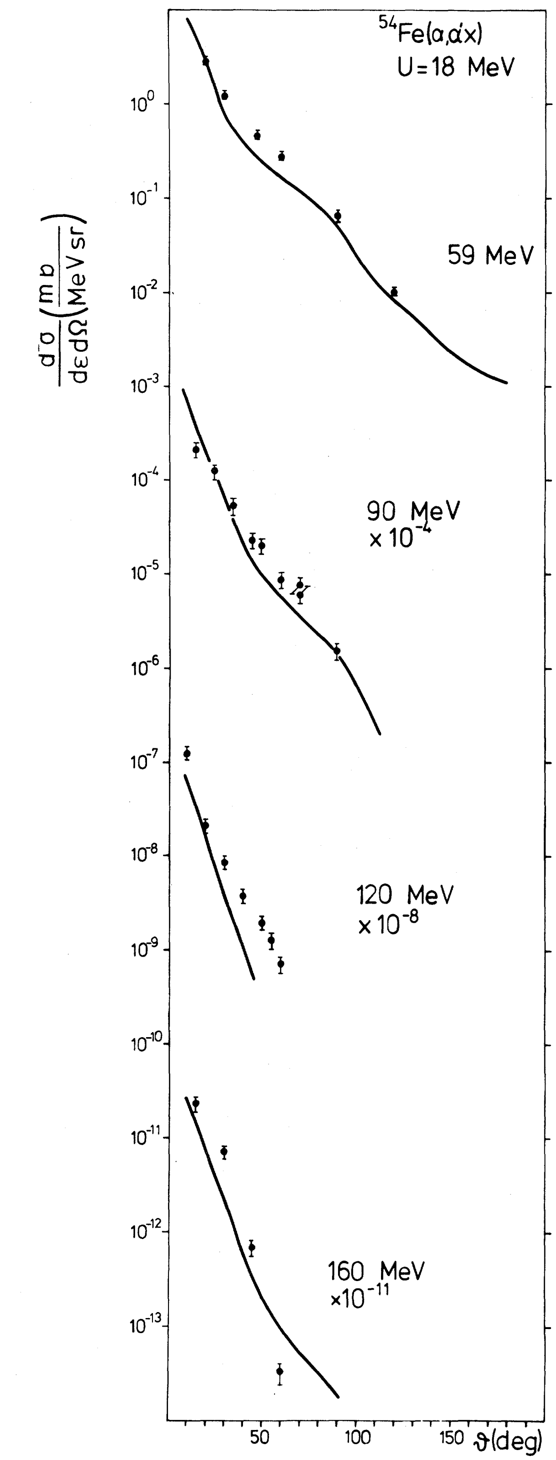

FIG. 15. As in Fig. 13, but the initial angular distribution $A(n_0\Omega)$ is given by Eq. (23).

where the rapidity plot showed the features discussed above. On the other hand, at fairly low excitation energies ECM yields the same results (dashed lines in Figs. 13 and 14) as Eq. (22). Angular distributions are shown in Figs. 13 and 14 for all energies under discussion. For these calculations the angular distribution function (7) has been used. While for 59 MeV bombarding energy the data could be nicely reproduced, the calculations fail more seriously as the bombarding energy is increased. A possible explanation for this effect might be that, for higher energies, the treatment of the nucleon-nucleon collisions in infinite nuclear matter and neglection of reflection and refraction at the nuclear surface are not valid approximations.

The experimental data, particularly in the forward angle regime, show a more exponential angular distribution. We, therefore, have tried an initial angular distribution

$$A(n_0,\Omega(\vartheta,\varphi))=a\exp(-b\vartheta) \tag{23}$$

to improve the quality of the model calculations. The normalization constant was obtained from the

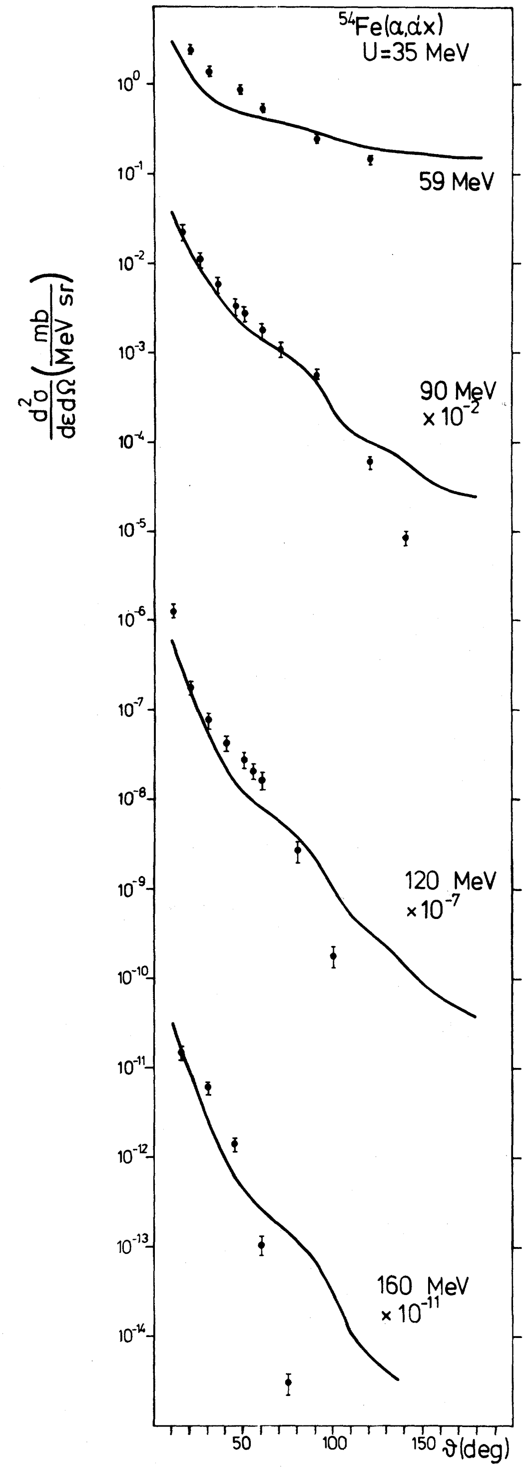

FIG. 16. As in Fig. 15, but for $U=35$ MeV.

Eq. (4). With $b=8$/rad we find the best agreement for all bombarding energies studied here and for all energies of the outgoing α particles. Comparisons of calculations using Eq. (23) with the data are given in Figs. 15–17. The agreement between calculations and data is excellent considering the simple underlying model assumptions.

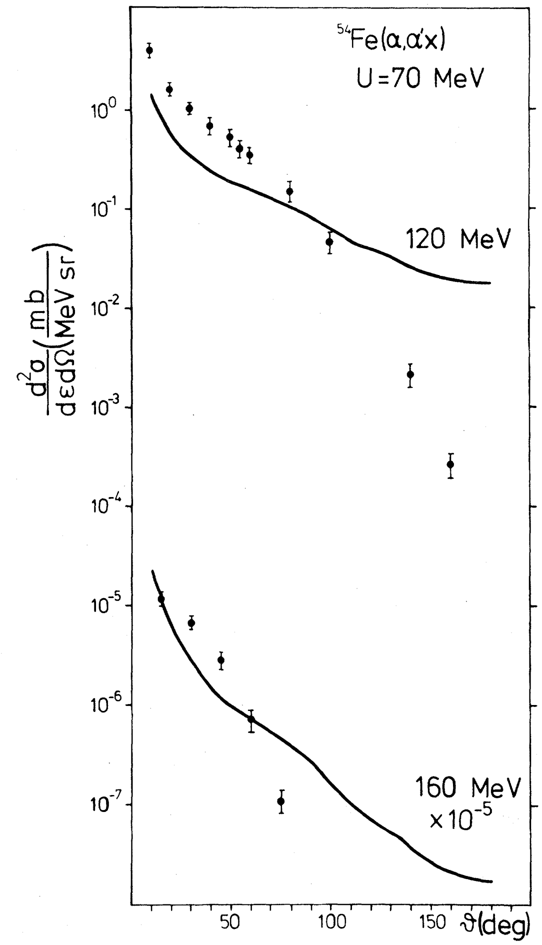

FIG. 17. As in Fig. 15, but for $U=70$ MeV.

In Fig. 18 angle-integrated data (dots) are compared with ECM calculations. Contributions of first-chance emission and second-chance emission following n, p, and α emission are shown. Obviously, the 59 MeV spectrum is dominated by first-chance emission α particles. For higher bombarding energies the importance of second-chance emission following n and p emission is observed. However, in all cases the contribution of second-chance emission following α emission is negligible. The absolute normalization of the spectra was obtained by adjusting the P_0 values compiled in Table II. They do, however, show a rather uniform behavior.

As mentioned in the Introduction, several approaches have been used in interpreting data from high energy heavy-ion induced reactions. Starting

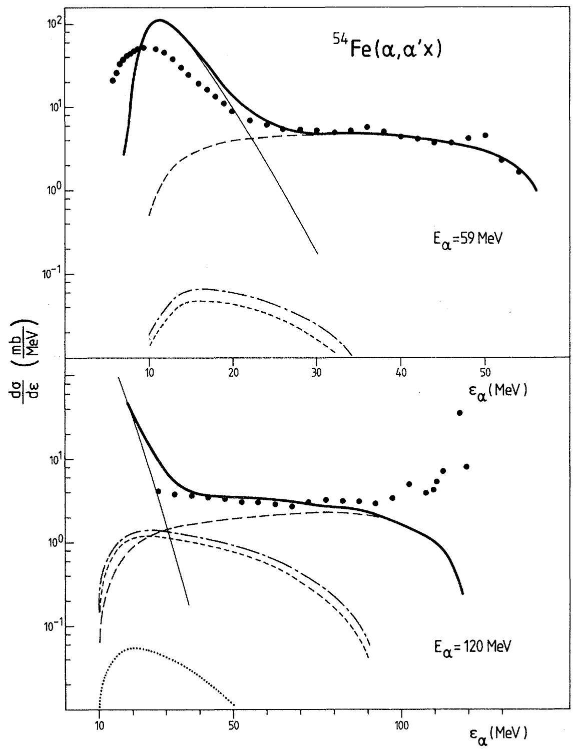

FIG. 18. Comparison of the angle integrated α' spectrum (dots) from the ^{54}Fe$(\alpha,\alpha' x)$ reaction at $E_\alpha=59$ and 120 MeV with ECM predictions taking only the first chance emission (long dashed curve) and the second chance emission following a neutron (dashed dotted curve), following a proton (short dashed curve), and following α emission (fine dotted curve at the bottom). The thin solid curve denotes the contribution from compound nucleus evaporation. The thick solid curve represents the sum of all contributions.

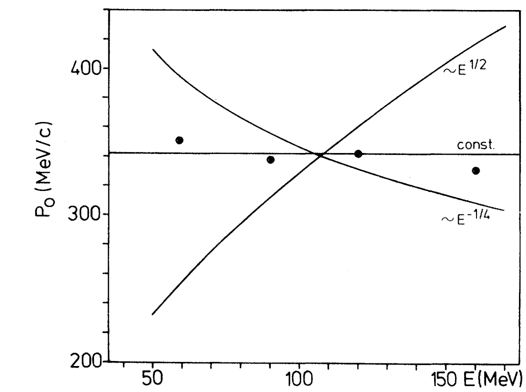

FIG. 19 Comparison of the extracted P_0 values (dots) with predictions of different models (see text).

from different physical assumptions these models lead to the same power law (20). However, they predict different energy dependences for P_0. We will not discuss the approaches in detail, since recent reviews[14,15] are available. We will give only the energy dependence of P_0, if a temperature T of the emitting system is calculated following an equation of state $T^2=(6/\pi^2 g)E$.

The sudden approximation[5] leads to $P_0 \sim E^{-1/4}$, an energy dependence also obtained in the statistical equilibrium approach.[4] Such a relation has been used in astrophysics for calculating the iron production in the e process[16] or in silicon burning,[17] $\alpha+{}^{28}\mathrm{Si}\rightarrow{}^{32}\mathrm{S}$.

Starting from statistical equilibrium and taking excited states of the composite particles into account, the energy dependence becomes[14] $P_0 \sim E^{1/2}$. However, due to the lack of the existence of excited states for light nuclei or the existence at high excitation energies (above 20 MeV for α particles) compared to the total excitation energy, this energy dependence must fail in the energy regime under discussion. In a pure final state interaction model the complex particle wave function in the rest frame of the system should not depend on the c.m. motion, i.e., P_0 = const. In Fig. 19 we compare the data for P_0 from the ECM analysis with the energy dependences given above. The functions for the energy dependences have been adjusted to reproduce the mean value of P_0 for the mean bombarding energy. In a recent paper[12] it has been shown that, from P_0, radii R in coordinate space could be obtained which are essentially those of the free clusters. For $R_\alpha=1.63$ fm a value $P_0=341$ MeV/c is obtained and indicated in Fig. 19 as a constant. By comparing the three different functional behaviors with the data, it becomes clear that $P_0=$ const is favored. As noted earlier this finding has been also obtained in relativistic heavy-ion induced reactions.[6]

V. CONCLUSION

It has been shown that angle-integrated complex particle spectra can be well reproduced by ECM, if multiple particle emission is properly taken into account. The assumption of free nucleon-nucleon collisions in infinite nuclear matter[10] fails for higher α-beam energies. An exponential angular distribution after the first projectile-target interaction nicely reproduces the data. By comparing energy dependences for the scaling factor P_0, as it is given from different model assumptions, we have determined that $P_0=$ const agrees best with the data. This finding favors a pure final-state interaction assumption for the cluster formation.

ACKNOWLEDGMENTS

We would like to thank Prof. C. Mayer-Böricke for critical and stimulating discussions. We are grateful to Dr. Yates for a carefull reading of the manuscript.

APPENDIX

In the following it is shown that complex particle emission from a moving thermal source shows the same source temperature T within the framework of CM as does nucleon emission.

We assume the isotropic emission of nucleons with mass u in the center of mass system (primed quantities) of a thermalized source. For a Maxwellian distribution the cross section yields (with the normalization constant, c)

$$\frac{d^2\sigma'}{d\epsilon'\,d\Omega'}=c\sqrt{\epsilon'}\exp(-\epsilon'/T)\ . \tag{A1}$$

Transformation into the laboratory system (unprimed quantities) for a source moving with velocity v_s parallel to the beam axis leads to

$$\frac{d^2\sigma(\vartheta)}{d\epsilon\,d\Omega}=c\sqrt{\epsilon}\exp[-(\epsilon-\sqrt{2u\epsilon}v_s\cos\vartheta+\tfrac{1}{2}uv_s^2)/T] \tag{A2}$$

for emission in direction ϑ.

Now CM [Eqs. (20) and (21)] is applied. In the following the mass of the complex particle with x protons and y neutrons is denoted by $m=(x+y)u$ and its kinetic energy is $E=(x+y)\epsilon$, if binding energy is neglected. When Eq. (A2) is inserted into Eq. (21) and then Eq. (21) into Eq. (20), the complex particle cross section is

$$\begin{aligned}\frac{d^2\sigma_{x+y}}{dE\,d\Omega}&=\frac{1}{x!y!}\left[\tfrac{4}{3}\pi P_0{}^3\frac{1}{\sigma_0\cdot u\sqrt{2u\epsilon}}\right]^{x+y-1}\left[\frac{d^2\sigma}{d\epsilon\,d\Omega}\right]^{x+y}\frac{1}{(x+y)^{3/2}}\\&=c^{x+y}(\tfrac{4}{3}\pi P_0{}^3/\sigma_0)^{x+y-1}\frac{1}{x!y!(x+y)^{3/2}}\left[\frac{1}{u\sqrt{2u}}\right]^{x+y-1}\\&\quad\times\sqrt{\epsilon}\exp[-(E-\sqrt{2mE}\cos\vartheta\cdot v_s+\tfrac{1}{2}mv_s^2)/T]\ .\end{aligned} \tag{A3}$$

Equation (A3) shows that complex-particle cross sections are again Maxwellian with the same features, such as velocity v_s and temperature T, as the emitting source.

[1]S. T. Buttler and C. A. Pearson, Phys. Lett. 1, 77 (1962).
[2]A. Schwarzschild and Č. Zupančič, Phys. Rev. 129, 854 (1963); Č. Zupančič, Phys. Lett. 4, 182 (1963).
[3]H. H. Gutbrod *et al.*, Phys. Rev. Lett. 37, 667 (1976).
[4]A. Mekjian, Phys. Rev. Lett. 38, 640 (1977); Nucl. Phys. A312, 491 (1978); Phys. Rev. C 17, 1051 (1978).
[5]R. Bond, P. J. Johansen, S. E. Koonin, and S. Garpman, Phys. Lett. 71B, 43 (1977).
[6]M. C. Lemaire, S. Nagamiya, S. Schnetzer, H. Steiner, and I. Tanikata, Phys. Lett. 58B, 38 (1979).
[7]J. Gosset *et al.*, Phys. Rev. C 16, 629 (1977).
[8]H. Machner, Phys. Lett. 86B, 129 (1979).
[9]G. Riepe and D. Protić, Nucl. Instrum. 101, 77 (1972).
[10]G. Mantzouranis, D. Agassi, and H. A. Weidenmüller, Phys. Lett. 57B, 220 (1975).
[11]G. Mantzouranis, Phys. Lett. 63B, 25 (1976).
[12]H. Machner, Phys. Rev. C 21, 2695 (1980).
[13]F. E. Bertrand and R. W. Peelle, Oak Ridge National Laboratory Report ORNL-4694, 1971 (unpublished).
[14]A. Mekjian, Phys. Lett. 89B, 177 (1980).
[15]J. I. Kapusta, Phys. Rev. C 21, 1301 (1980).
[16]E. M. Burbridge, G. R. Burbridge, A. Fowler, and F. Hoyle, Rev. Mod. Phys. 29, 547 (1957).
[17]D. Bodansky, P. D. Clayton, and W. A. Fowler, Astrophys. J. Suppl. Ser. 148, 16, 299 (1968).